Advances in Environmental Technology 10(4) 2024, 339-359.

Iranian Reasearch Organization for Science and Technology (IROST)

Advances in Environmental Technology

Journal home page: https://aet.irost.ir

Synthesis of hydroxyapatite-zeolite from blast furnace slag and its application for the removal of copper, lead and copper-lead mixture by adsorption

Toufik Chouchane*[a], Mohamed Tayeb Abedghars[a], Sabiha Chouchane[b], Atmane Boukari[a]

[a] Research Center in Industrial Technologies CRTI, P.O. Box 64, Cheraga 16014 Algiers Algeria.
[b] Faculty of Sciences, Badji Mokhtar University, Annaba Algeria.

ARTICLE INFO

Document Type:
Research Paper

Article history:
Received 20 July 2024
Received in revised form
22 October 2024
Accepted 27 October 2024

Keywords:
Adsorption
Copper
Lead
Slag
Hydroxyapatite-Zeolite

ABSTRACT

This article sheds light on the applications of hydroxyapatite-zeolite (HZ) from a steelmaking by-product, namely treated blast-furnace slag (TBFS), in the adsorption of copper, lead and copper-lead mixture in batch mode. Chemical and spectral analysis showed that sodium oxide, silicon dioxide, aluminum oxide, calcium oxide, and phosphorus hemi-pentoxide are the main constituent elements of HZ. After conversion of TBFS to HZ, the specific surface area experienced a significant expansion from 275.8 to 409.63 m2/g, while the point of zero charge (PZC) regressed from 3.8 to 3.4 on the pH scale. The sodium oxide/alumina, lime/phosphorus pentoxide, and silica/alumina ratios, estimated at 1.71, 1.61, and 1.31, respectively, indicate that the slag was transformed into hydroxyapatite-zeolite. The tests revealed that the impact of contact time (50 min), HZ mass (1g), solution agitation (200 rpm), solution pH (5), medium temperature (20 °C), HZ particle size (250µm) and initial concentration of the pollutant solution (240 mg/L) significantly improved the efficiency of these processes, where the adsorption power of copper, lead and mixture reached 124.87 mg/g, 115.14 mg/g and 108.74 mg/g, respectively. The adsorption isotherms demonstrated that the processes in question occurred on a homogeneous surface covered with a single layer, as evidenced by the correlation coefficients and the capacities of adsorption. The kinetic models demonstrated that the sorption processes undertaken obeyed pseudo-second-order kinetics ($R^2 \geq 0.99$). Examination of the adsorption mechanism highlighted that these processes are regulated by various external and internal diffusions. Thermodynamic evaluations confirmed that ongoing procedures are characterized by heat release (exothermic). In addition, they demonstrate their spontaneous character, which is less disordered and results from physical interactions (physical adsorption). It has been demonstrated by the desorption process that HZ can be reused for 6 successive cycles.

*Corresponding author Tel.: +213661111070
E-mail: chouchane_toufik@yahoo.fr
DOI: 10.22104/aet.2024.6914.1893

1 Introduction

Water pollution by metals presents a major concern for humans and their ecosystems given that they are toxic, harmful and non-biograbable [1]. The accumulation of metals in the body leads to terrible consequences. Indeed, in living beings, they can exert an influence on the nervous, renal, respiratory, cardiovascular and digestive systems [2]. In addition, they can pollute the soil and thus compromise plant growth [3]. In order to slow down and then curb this terrifying disaster, innovative and effective techniques have been designed, such as physicochemical treatments, treatments using membranes, ion exchange treatments, and also adsorption [4,5]. Due to its performance and simplicity, adsorption was chosen as the treatment of choice among the available techniques. In addition, it requires less energy and generates less sludge [6,7]. Consequently, we favoured the adsorption technique. Copper and lead, in their Cu(II) and Pb(II) forms, respectively, were used like adsorbates, while hydroxyapatite-zeolite (HZ) synthesized from treated blast furnace slag (TBFS) was employed as an adsorbent.

Copper is one of the least toxic heavy metals; its presence in excess is harmful, although it is an important nutrient [6]. Lead is classified among the most harmful metals, and it is extremely dangerous, even in small quantities [4,8]. These two metals, to varying degrees of harm, are capable of causing irreversible damage to man and his environment, accumulating in the vital organs of living beings and in the food chain [8-10]. The most common sources of water contamination by these metal ions are water emissions from mining operations and industries such as steel, metallurgical, fertilizer production, metal surface treatments, paint production, metallurgical manufacturing, plastic, etc. [6,7,11]. According to the literature, it has been cited that the elimination of lead(II) and copper(II) ions in solution has been carried out via a number of adsorbents, namely agricultural waste [12,13], clay [14,15], nanomaterials [16,17], nanocomposite [18,19], and carbon-based adsorbents [20,21].

The examined adsorbent (HZ) was prepared from TBFS, obtained from raw blast furnace slag. Generally speaking, steel slags are used in building construction [22], in public works [23], and in soil stability [24]. Due to a colossal global annual production of 300 million tonnes, this product is likely to cause considerable financial losses as well as environmental damage due to prolonged storage outdoors. With this in mind, we have recently focused our efforts on the valorization of this substance in the adsorption process in an aqueous medium. Effectively, we used treated TBFS in various solution adsorption processes, such as the adsorption of nickel [22], lead [7], manganese [23], copper [6], and trivalent chromium [24].

Following technological development and the progression of applied research, slag derivatives have taken on another dimension in the wastewater treatment sector. Indeed, numerous literary researches have highlighted the use of slag derivatives during adsorption processes. We observed that NaA zeolite and silica nanoparticles prepared from blast furnace slag were used effectively in the removal of methylene blue by adsorption [25,26]. Furthermore, basic oxygen furnace slag modified by mechanochemistry, oxalated blast furnace slag, and metaettringite synthesized were used in the adsorption of copper, cobalt, and boron, respectively [27-29].

The aim of this work is to present a reliable adsorbent at reasonable prices to contribute to the birth of a venerable and sustainable environment. The approach adopted in this study is to valorize TBFS by converting it into HZ zeolite to create additional adsorption sites and, consequently, to improve its adsorption power. The conversion of TBFS to HZ was accomplished following chemical and thermal treatment. The TBFS and HZ solids were examined using X-ray fluorescence (XRF) and X-ray diffraction (XRD). The adsorption process was carried out in batch mode under the influence of determining factors. Research has been conducted on adsorption isotherms, adsorption kinetics and thermodynamic analysis. It is important to note that blast furnace slag and its derivatives can be used without difficulty in water decontamination. Moreover, they are more economically profitable than commercial adsorbents.

2. Materials and methods

2.1. Treatment of solid adsorbent

The slag solid samples were collected from the Annaba steel factory, Algeria. It was treated in accordance with the experimental approach presented in multiple research works [7,21]. This experimental protocol was established using the following methodology:

- The collected slag was cleaned with distilled water and dried in air for two days (48 hours).
- After being cleaned, the slag samples were powdered and sorted by size: 50, 150, 300, and 450 µm.
- The slag samples, from the last operation were again individually cleaned with distilled water, before being steamed at 105°C. After steaming, they were saved in plastic boxes

In accordance with the studies carried out [25,26,30-33], we sought to minimize the quantity of lime while increasing the quantity of silica and alumina. Our objective was to produce hydroxyapatite-zeolite from treated blast furnace slag. Hereinafter is provided a concrete illustration of the operating protocol executed during the experiment.

- In a one liter beaker, we incorporated 50 grams of treated slag into a solution of caustic soda at a concentration of 1M. Subsequently, the prepared solution was stirred and heated at the same time at a speed of 200 rpm and a temperature of 80 °C. This stage lasted 4 hours.;
- The solid formed during the previous procedure was separated and collected, following a waiting period of approximately 120 minutes, using a filtration process.
- The collected solid was heated at 850°C for 2 hours, then inserted into a solution containing Na_2HPO_4 (10 mg/L). After carrying out this operation, we gently mixed the preparation at a speed of 100 rpm until a homogeneous mixture was obtained.
- Over a period of 5 minutes, drops of 0.1M NaOH were gradually added to the homogenized solution while stirring, then it was left to stand until the solid had completely dissociated from the liquid.
- The new material was collected by filtration and washed with distilled water, air dried for 4 hours, and then subjected to oven drying at 105°C for a dozen hours straight before be stored in appropriate containers.

2.2. Equipment and reagents

The Perkin Elmer 3110 atomic absorption spectrometer was used to analyze copper and lead ions. The analysis of the chemical composition of the slag and the HZ zeolites was carried out using the Siemens SRS 3000 Spectrometer using X-ray fluorescence, while the spectral analysis was carried out with the Rigaku Ultim IV Diffractometer using X-ray diffraction. X-rays. The pH value was evaluated using a high-quality Ericsson pH meter. The heating operation of TBFS and HZ was carried out in a Nabertherm model HT16/17 muffle furnace. Agitation of the solutions studied was performed by mechanical stirrer operating at multiple speeds. The evaluation of the mass area, also referred to as specific surface area, of the TBFS and the HZ was measured thanks to the Brunauer, Emmett, and Teller model. The reagents used, namely hydrochloric acid (HCl), sodium hydroxide (NaOH), copper(II) nitrate ($Cu(NO_3)_2$* $3H_2O$), and lead(II) nitrate ($Pb(NO_3)_2$* $6H_2O$) were of analytical grade (Merck). While sodium hydrogen phosphate (Na_2HPO_4) is from Haltichem. Blast furnace slag from the Annaba steel complex, Algeria

2.3. Specific surface determination

The specific surface area was evaluated by measuring the amount of nitrogen absorbed, corresponding to the pressure to which it was subjected. This method is based on the principle of gas adsorption at low temperatures to determine the total surface area of a solid sample without altering its structure. The Van der Waals forces at the surface of the solid are at the origin of this process, exerting their action on the gas molecules surrounding the solid sample. This experiment was carried out at a temperature of -196 °C and under a pressure equivalent to the standard atmospheric pressure of 760 mmHg [23,34]. The nitrogen gas desorption results were interpreted using a specific model, namely the BET model [19,35].

2.4. Point of Zero Charge

The pH in agreement with the PZC was evaluated based on the experiment previously carried out by our

team. For these experiments, we used 1 gram of HZ, with a particle size of around 300 µm, and potassium chloride (KCl) solutions at 0.1 and 0.01M [5,7,24]. It should be specified that the volume of the solution is 100 ml. The PZC specification is important because it tells us about the type of charge present on the surface of the solid under examination (positive, neutral, or negative) [4,12].

2.5. Adsorption process

A series of tests were carried out to examine the adsorption of copper, lead, and the lead-copper mixture in an aqueous medium by the zeolite in batch mode. The examined metal ion solutions (Cu, Pb, and Cu-Pb) were prepared using copper(II) nitrate trihydrate ($Cu(NO_3)_2$ * $3H_2O$) and lead(II) nitrate ($Pb(NO_3)_2$ * $6H_2O$). The volume of the solutions used is 1 liter. The mixture is composed of equivalent concentrations of copper and lead. The experimental method involved adding a certain amount of zeolite into a solution containing the pollutants targeted for analysis. The experimental methods described in the literature have been employed to properly conduct our experimental approach [5,6,22,24]. Factors such as contact time (t_c), adsorbent mass (m_s), stirring speed (V_{ag}), solution temperature (T), solution pH, solid grain size ($Ø_s$), and concentration of pollutant solution (C_0) have been adjusted to maximize their efficiency, and therefore perfect the processes carried out. Experimental conditions are displayed in Table 1.

Evaluations of the adsorbed quantity (q_e), equilibrium residual concentration (C_e), and adsorption percentage (%R) were carried out based on equations 1, 2 and 3.

$$q_e = \frac{C_0 - C_t}{m} \times V \quad (1)$$

$$C_e = C_0 - C_t \quad (2)$$

$$\%R = \frac{C_0 - C_e}{C_0} \times 100 \quad (3)$$

Where C_0, C_t, and C_e: starting concentration, concentration measured at time t, and concentration measured at equilibrium (mg/L).

2.6 Desorption process

The HZ reuse study was investigated using HCl, H_2SO_4 and HNO_3 as eluents at 0.05 M. This work was performed following the method suggested by Chouchane et al. [6]. The description of the experimental conditions is as follows:

- 20 g of saturated HZ were obtained by filtration using a filter paper.
- The recovered HZ was incubated for 24 hours at 105°C.
- Desorption was completed after 60 minutes of contact under moderate stirring of the order of 250 rpm

Table 1. Detailed specifications for each stage of the experiment

Steps	Parameter values
Impact of t_c	t_c: 0-180 min; m_s: 1 g; V_{ag}: 150 rpm; T: 20 °C; pH: 4.5; $Ø_s$: 500 µm; C_0: 30 mg/L
Impact of m_s	t_c: 50 min; ms: 0.4, 0.6, 0.8, 1, 1.2, and 1.4g; V_{ag}: 150 rpm; T: 20°C; pH: 4.5; Øs: 500 µm; C_0: 30 mg/L.
Impact of V_{ag}	t_c: 50 min; m_s: 1 g; V_{ag}: 50, 100, 150, 200, and 250 rpm; T : 20 °C; pH: 4.5; $Ø_s$: 500 µm; C0: 30mg/L
Impact of T	t_c: 50 min; ms : 1g; V_{ag}: 200 rpm; T: 20, 35, 45, and 55 °C; pH: 4.5; $Ø_s$: 500 µm; C_0: 30 mg/L;
Impact of pH	t_c: 50 min; m_s: 1 g;V_{ag}: 200 rpm; T: 20°C; pH: 2.6, 3.2, 4, 4.5, 5, and 5.4; $Ø_s$: 500 µm; C_0: 30 mg/L
Impact of $Ø_s$	t_c: 50 min; m_s: 1g; V_{ag}: 200 rpm; T: 20 °C, pH: 5; $Ø_s$: 150, 250, 500, 800 µm; C_0: 30mg/L
Impact of C_0	t_c: 50 min; m_s: 1 g;V_{ag} : 200 rpm; T: 20°C; pH: 5;; $Ø_s$: 250µm, C_0: 30-300 mg/L

3. Results and discussion

3.1. Description of the analyzed adsorbent

Experimental data from physicochemical verification (XRF and XRD) of blast furnace slag samples are in harmony with information previously published in the literature [7]. According to Table 2, the slag was mainly formed of silica (SiO_2), representing 40.1%; lime (CaO), with a content of 35.45%,; alumina (Al_2O_3) at 12.96%; and magnesium oxide (MgO), for 5.12%. In Figure 1a, we noticed that the results obtained using the XRF analysis are in agreement with those of the XRD analysis. Examination of the modified slag showed

that it is mainly composed of sodium oxide (Na_2O with a content of 27.11%), silica (SiO_2 with a content of 20.74%), alumina (Al_2O_3 with a content of 15.78%), lime (CaO with a content of 11.65%), and phosphorus pentoxide (P_2O_5 with a content of 7.28%) (Table 2). Peaks concordant with sodium oxide, silica, alumina, lime and phosphorus pentoxide were identified by XRD examination (Figure 1b), which made it possible to affirm the results obtained by XRF. The calculated Si/Al, Na/Al, and Ca/P ratios are 1.31, 1.71, and 1.61, respectively. These evaluations highlighted that the TBFS was converted to a hydroxyapatite-zeolite [33]. The significant variation in the percentage of sodium oxide (Na_2O) can also be seen as another indicator of the transformation of TBFS into HZ. Considering these results, we came to the conclusion that the slag transformed into hydroxyapatite-zeolite, where zeolite is formed from Na_2O, SiO_2, and Al_2O_3, while hydroxyapatite is composed of P_2O_5 and CaO [33,36]. Minor metal ions are not visible in Figure 1b. This is probably due to their dispersion in the HZ structure. [37-39].

Table 2. Chemical composition of treated slag [21], and modified slag (HZ)

Element	Mass %	
	Slag	HZ
CaO	35.45	11.64
Al_2O_3	12.96	15.78
SiO2	40.1	20.74
Fe_2O_3	2.11	0.82
MgO	5.12	1.02
MnO	1.04	0.4
K_2O	0.2	0.21
Na_2O	0.7	27.11
P_2O_5	0	7.27
LOI	2.32	14.98

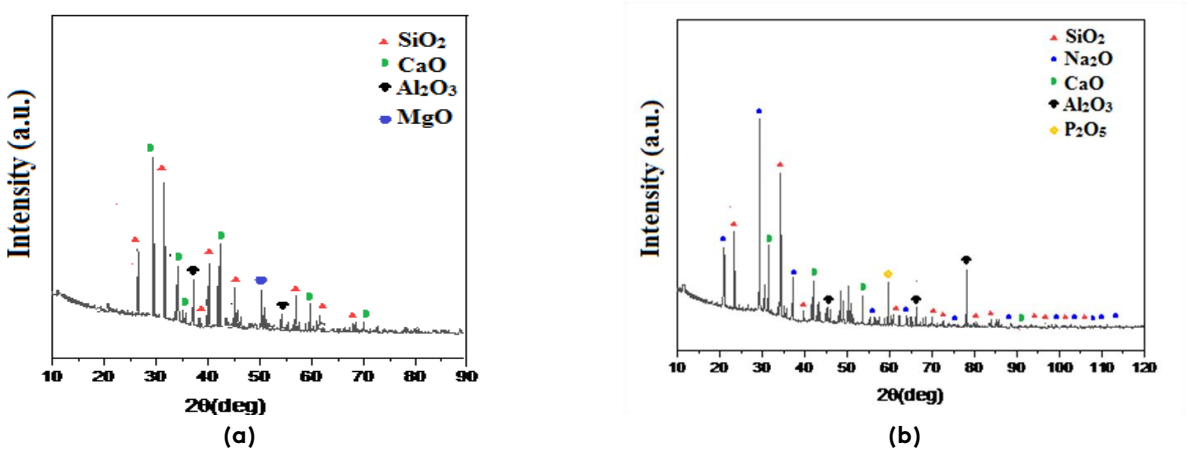

Fig. 1. Diffractogram: (a) Blast furnace slag [7], (b) hydroxyapatite-zeolite (HZ)

The characterization examination of the adsorbent surface of the TBFS and the HZ revealed that the specific surface a increased by 133.83 m^2/g (TBFS specific surface = 275.8 m^2/g [22], and HZ specific surface = 409.63 m^2/g) (Figure 2). This result revealed that the conversion of TBFS to HZ generated new adsorption sites, which will surely contribute to better adsorption. It is worth mentioning that the formation of hydroxyapatite and zeolite of the new HZ material occurs in several phases. First, the nucleation of hydroxyapatite and zeolite occurs in parallel, with the development of hydroxyapatite crystals prevailing, while most of the silicon and aluminum constituents remain in amorphous form. It is highly likely that the crystalline progression of hydroxyapatite is the result of a lower activation energy for the nucleus, combined with a limitation of this zeolite nucleus due to the participation of calcium in the reaction scheme [33]. Secondly, calcium is fully exploited by phosphorus, causing the creation of hydroxyapatite crystals. At the same time, the silicon and aluminum ions of the slag depolymerize in alkaline solution, and the nucleation of the zeolite occurs, thereby triggering an increase in sodium in the solid phase [31,36]. The development of the hydroxyapatite-zeolite crystal occurred following polymerization and depolymerization mechanisms at the interface of the solid and liquid phases [33,37].

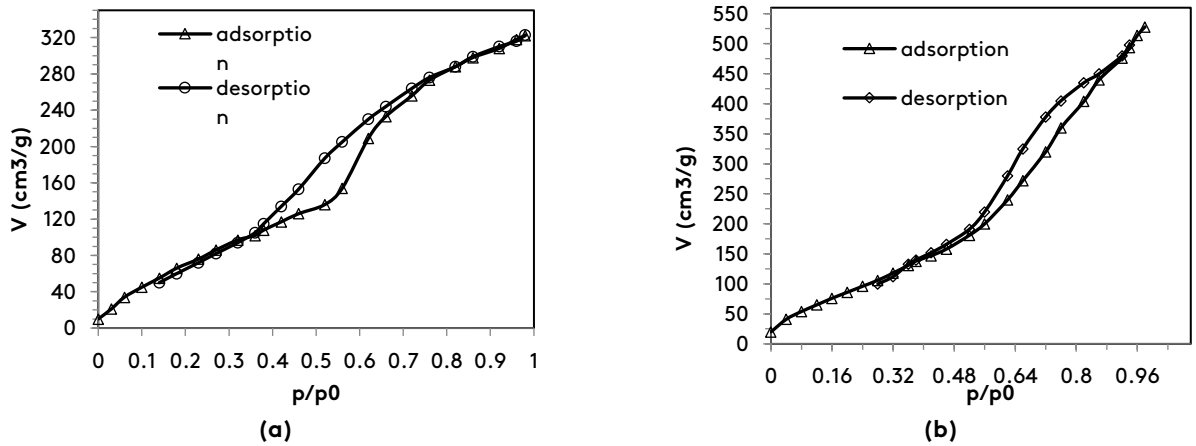

Fig. 2. (a) N_2 adsorption-desorption isotherm of TBFS , (b) N_2 adsorption- desorption isotherm of HZ

3.2 Effect of contact time

The graphic illustration in Figure 3a explicitly describe the impact of contact duration on the adsorption processes of the pollutants discussed, including Cu(II), Pb(II) and Cu-Pb. In accordance with experimental data, it was spotted that the adsorbent surface of HZ reached its maximum capacity after 50 minutes during the adsorption of the evoked ions previously (copper, lead, and copper-lead). From Figure 3a, the adsorption of copper(II) and lead(II) ions was considerable and rapid for the first 20 min, before gradually attenuating until the saturation of the HZ active surface after 50 min of contact. It is very likely that the high sorption rate of Cu(II) and Pb(II) ions is caused by the interactions created between the pollutants examined and the many accessible adsorption sites on the surface of the HZ, generated by strong forces of attraction [5]. The deceleration of adsorption between 20 and 50 min was certainly caused by the gradual lowering of the available adsorption sites, and the interruption of the adsorption processes was necessarily due to the saturation of the adsorption surface [7,22]. However, the adsorption of the binary mixture (Cu-Pb) proceeded at an almost similar rate until the process was interrupted, as shown in Figure 3a. It is highly probable that the competition effect between the copper and lead ions in the solution induced this outcome.

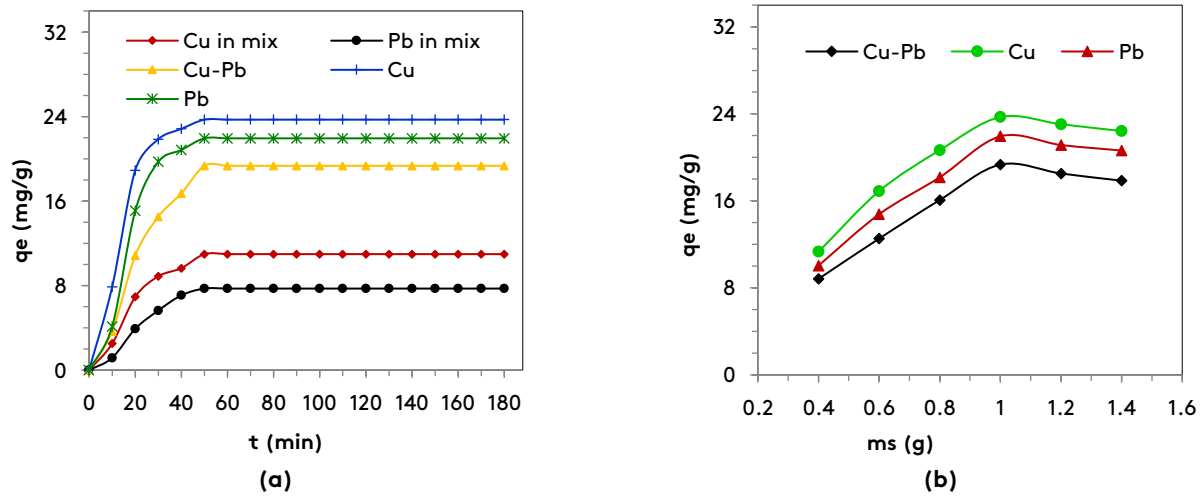

Fig. 3. (a) Impact of contact time on adsorption processes, (b) Adsorption capacity of HZ zeolite at equilibrium as a function of various masses

3.3 Effect of HZ mass

The relationship between the mass and the adsorption of examined metal pollutants was investigated by increasing the mass from 0.4 to 1.4 g, as depicted in Figure 3b. The experimental trials have attested that the processes debated achieve their optimal efficiencies for a mass of 1 g. It was

noted that the removal capacity of copper increased from 8.83 to 19.34 mg/g, as did that of lead, which increased from 11.32 to 23.71 mg/g, and that of the mixture, which increased from 10.05 to 21.94 mg/g. We noticed also that the removal rate improved between 52.96 and 79.03% for copper, 49.23 and 73.13% for lead, and 41.76 and 64.46% for the mixture. The evolution of the adsorption processes between 0.4 and 1 g is clearly explained by the appearance of many unoccupied locations on the surface of the HZ [40,41]. It is most likely that the reduction in adsorption efficiency for masses greater than 1 g is caused by insufficient metal ions in solution, as adsorption sites continue to advance [42,43].

3.4 Effect of agitation speed

As part of these experiments, the processes carried out were subjected to a variety of stirring speeds, ranging from 50 to 250 rpm, as evident in Figure 4a. According to the data obtained, it was established that the adsorption efficiency evolved proportionally to the stirring speed, between 50 and 200 rpm, as represented in Figure 4a. Indeed, the adsorption capacity and removal percentage clearly increased by 10.95 mg/g and 36.5%, 10 mg/g and 33.3%, as well as 10.46 mg/g and 34.84%, respectively for copper (II), lead (II) and the mixture. It is very likely that the uniform distribution of the HZ in the medium and the intensification of the diffusion coefficient are at the origin of the exceptional results observed [44,45]. Figure 4a disclosed that at a rhythm of 200 rpm, the sorption capacity of copper(II), lead(II) and copper-lead ions remains unchanged. The interruption of external diffusion is a direct result of the removal of the liquid barrier from the mass and, consequently, the end of the adsorption process [6,22].

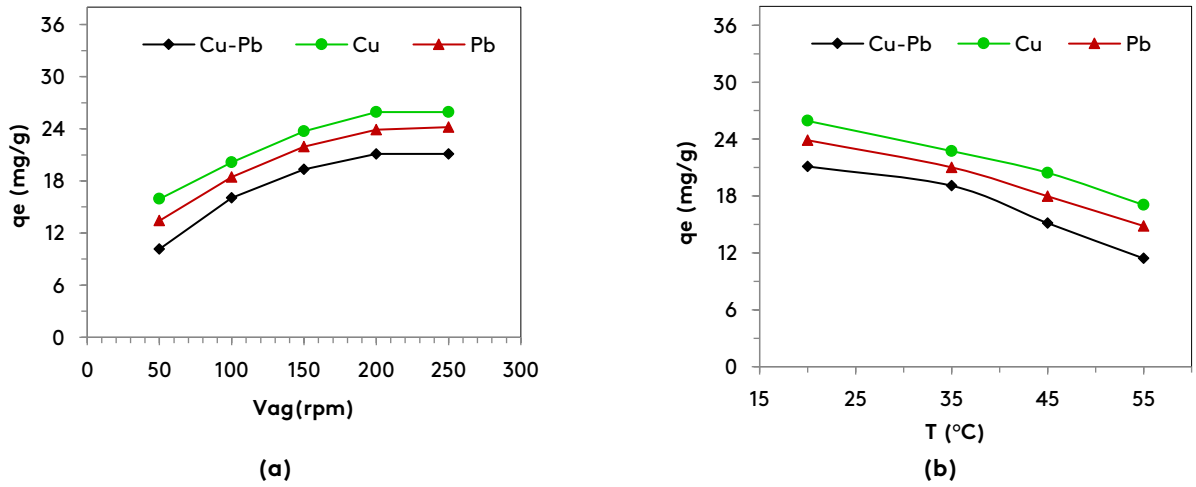

Fig. 4. (a) Impact of agitation speed, (b) Effect of temperature

3.5 Impact of the medium temperature

Study of the impact of medium temperature on the sorption of specific pollutants, including copper(II), lead(II), and copper-lead mixture, was carried out at a variety of temperatures, as presented in Figure 4b. According to the experimental approach performed, we observed that the performance of the sorption operations carried out decreased as the temperature of the medium intensified. Between 20 and 55 °C, the amount of Cu(II) removed decreased by 8.86 mg/g, as did that of Pb(II), which decreased by 9.04 mg/g, and that of the Cu-Pb mixture, which has regressed by 9.69 mg/g. The calculation results showed a 29.53% decrease in the adsorption rate of Cu(II), a 30.13% decrease for Pb(II) and a 32.3% reduction for the copper-lead mixture. The involution of the sorption of copper (II), lead (II) and the copper-lead mixture was apparently caused by the lowering of the electrostatic interactions between the adsorbates and the absorbent surface of HZ. Effectively, the growth in temperature of the aqueous medium caused a multiplication in the mobility of metal pollutants, thus leading to this phenomenon, that is to say drop in yield [46]. Given this result, it seems likely that the sorption of Copper(II), lead(II), and the copper-lead mixture on HZ causes

a release of heat, which means that the process is exothermic [1,47-49].

3.6 Impact of initial pH

In this stage of study, we examined these processes by subjecting them to pH measurements ranging from 2.6 to 5, as shown in Figure 5b. To simplify our work and improve our understanding of the adsorption process, we determined the PZC and restricted our analysis to a pH of 5, taking into account the fact that precipitation of copper(II) into copper hydroxide starts at 5.1 on the pH scale [13,21].

The experiments performed determined that the pH for a zero-charge surface is approximately 3.6 (PZC), as shown in Figure 5a. This outcome highlighted the different charge states of HZ zeolite. In other words, the zeolite surface is positive when the pH is less than 3.6, negative when the pH is greater than 3.6, and chargeless when the pH is equal to 3.6 [5,38]. This means that the most suitable medium for these processes is above pH 3.6. From Figure 5b, we noticed the reaffirmation of what was previously cited. Indeed, it has been observed that the sorption of copper (II), lead (II) and the mixture begins to improve at pH 4, and that it is maximum when the pH is equal to 5. The considerable performances of the sorption processes at pH ≥ 4 is certainly due to the intense interactions between the ions of copper, lead and the copper/lead mixture carrying positive charges and the surface of the HZ zeolite carrying negative charges [7,50]. Research has highlighted that the involution and unfavorability of the performance of the processes as we have discussed them (pH < pHpzc) is caused by the appearance of electrostatic repulsive forces between HZ zeolite and dissolved metal ions [5,15,37,51]. The inefficiency observed at pH ≤ 3.2 was also due to the presence of several protons interacting with the ions examined [26,38,49].

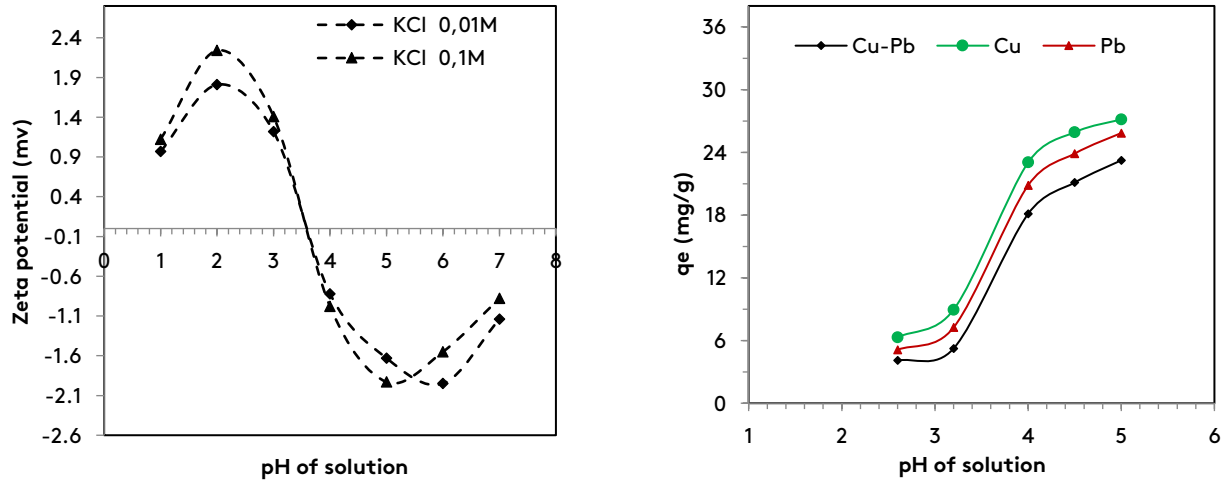

(a) (b)

Fig. 5. (a) Zero Charge Point Evaluation, (b) Effect of pH

3.7 Effect of particle size

It is generally recognized that the grain size of solids, such as HZ, has a major incidence on mass transfer during adsorption processes [6,24]. In order to achieve this objective, we analyzed the sorption of copper(II), lead (II), and the copper-lead mixture as a function of particle sizes (Øs) of 150, 250, 500, and 800 µm, as shown in Figure 6a. Based on experimental data, we noticed a clear improvement in the sorption of Cu(II), Pb (II), and Cu-Pb whenever the particle diameter was decreased from 800 to 250 µm. Effectively, the adsorption capacity has progressed from 4.26, 4.04 and 3.74 mg/g for copper, lead and the mixture, respectively. Calculations revealed an increase in the adsorption rate during the removal of copper (II), lead (II) ions and the copper-lead mixture, with respective values of 5.83, 4.9, and 4.76 %. Decreasing the particle size from 800 to 250 µm increased the adsorption surface area, which resulted in an increase in adsorption efficiency [52,53]. From Figure 6a, it was found that adsorption was less efficient for particles whose

diameter did not exceed 150 µm. The drop in adsorption efficiency is most certainly caused by the grouping of the grains of the solid (coalescence or agglomeration phenomenon) [45]. During this manipulation, the particles of the solid expand, thus causing a reduction in its adsorbent surface area [52].

3.8 Impact of Variation in Solute Concentration

For the purpose of completing the improvement of the proposed sorption process and drawing the experimental isotherms, we examined the influence of the concentration of the solution between 30 et 300 mg/L, as revealed in Figure 6b. The experiments demonstrated that the sorption of copper (II), lead (II) and the mixture of the two developed in a similar manner. At first, the processes showed steady growth, but then remained unchanged, unaffected by the addition of metal ions, see Figure 6b. The increase in sorption capacity can be assigned to the creation of a considerable driving force, promoting the movement the addressed pollutants from solution to the surface of HZ and simultaneously decreasing the resistance to exchange massive. Due to the unavailability of sorption sites on the HZ, the adsorption is interrupted, resulting in straight lines on the graph (Figure 5b), suggesting that the HZ has reached its maximum capacity [6,22]. Adsorption capacity of copper (II), lead (II), and the copper-lead mixture were 124.87 mg/g, 115.14 mg/g, and 108.47 mg/g, respectively. It is highly likely that the competition between copper(II) and lead in the mixture was responsible for the reduction in the adsorption capacity of the mixture, compared to mono-adsorption [24,54,55]. The adsorbed amounts of copper and lead in the mixture individually corresponded to 65.45 mg/g and 43.02 mg/g, which showed that HZ has more affinity for copper, even though its hydrated ionic radius (0.419 nm) is slightly larger than that of lead (0.401 nm) [56].

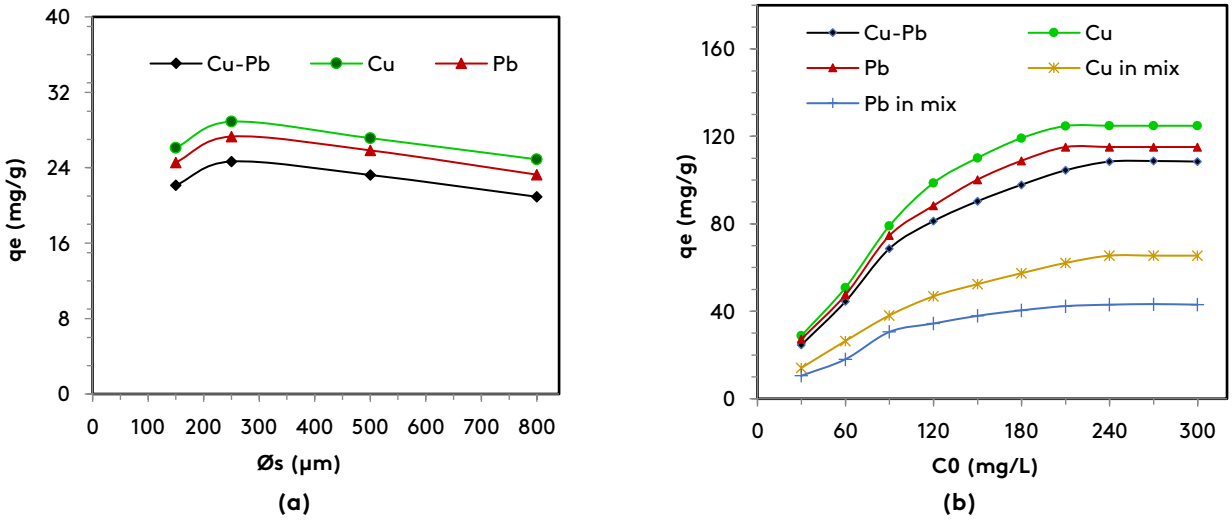

Fig. 6. (a) Impact of particle size ($Ø_s$), (b) Impact of Initial Concentration (C_0)

Based on equation 3, we observed that the adsorption yield of copper (II), lead(II) and copper-lead mixture diminished as the initial concentration increased. The percentage reduction in yield for the adsorption of copper (II), lead (II), and copper-lead mixture was 54.67%, 52.65%, and 46.04%, respectively. Effectively, by increasing the initial concentration while maintaining the same characteristics of the adsorbent, this causes an increase in the residual concentration of the metal ion in solution, thus causing a reduction in the percentage of elimination [7,24]. It is essential to emphasize that HZ prepared from slag of blast furnace demonstrated significant adsorption power (Table 3).

As mentioned earlier, the removal of metal ions on HZ was found to be more efficient at pH 5, where the adsorbent surface of HZ has a negative charge, as opposed to pollutants, which carry positive charges. This effect played a considerable role in the adsorption of copper, lead, and copper-lead mixture by HZ, due to the electrostatic interactions present. In Figure 6, we have presented, as an example, the adsorption of copper on HZ, since the fixation systems are similar for the three adsorbed processes.

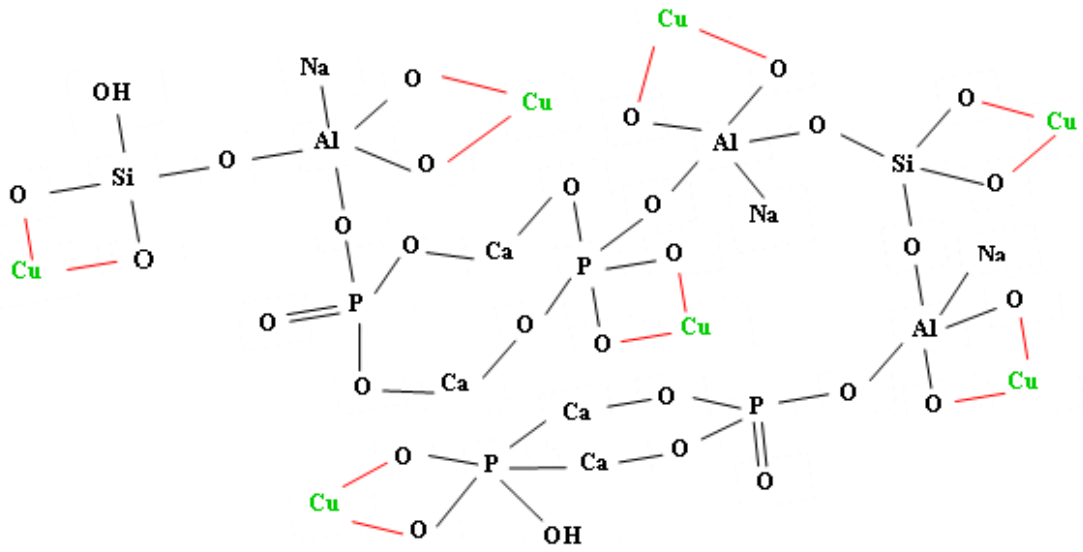

Fig. 7. Copper fixation system on the adsorbent surface of HZ

Table 3. Adsorption capacities of copperr(II) and lead (II) by various adsorbents.

Adsorbents	Ions	qe, *(mg/g)*	Ref.
biochars	Cu	223	[4]
Blast furnace slag		45.16	[6]
Nanofibers-clay mineral		87	[15]
Olive branches activated carbon		43.10	[20]
kaolin		46.18	[49]
Groundnut husk		33.49	[57]
softwood and hardwood biochars		23.42	[58]
Current study		124.87	
Composite material	Pb	196.35	[10]
Activated Aloji clay		166.66	[14]
Iron oxide nanomaterials		97.5	[16]
Carbon nanotube composites		83.20	[18]
Blast furnace slag		50.12	[24]
kaolin		35.69	[55]
Cellulose acetate		70.5	[59]
Tobacco leaves		24.7	[60]
current study		115.14	

3.9 Examination of Adsorption Isotherms

To highlight the interactions between HZ and the metal pollutants in question, we used mathematical models commonly recognized in sorption processes, including Freundlich, Langmuir and Temkin [61]. The considered models are represented by equations 4 to 6.

$$\ln q_e = \ln k_F + \frac{1}{n}\ln C_e \quad (4)$$

$$\frac{C_e}{q_e} = \frac{1}{q_{max}} C_e + \frac{1}{q_{max} b} \quad (5)$$

$$qe = B_T \ln A_T + B_T \ln Ce \quad (6)$$

Where q_e and q_{max}: experimental adsorption capacity and maximum theoretical adsorption capacity (mg/g), C_0 and C_e are: initial concentrations and concentration measured at equilibrium (mg/L), b: Langmuir isotherm constant (L.mg-1), R_L: one-dimensional parameter named separation factor, k_F: Freundlich isotherm constant, 1/n: heterogeneity factor, $B_T = \frac{RT}{b_T}$, A_T : Temkin isotherm equilibrium binding constant

(L/g), b_T : constant related to heat of sorption (kJ $kmol^{-1}$).

Freundlich, Langmuir, and Temkin models plots are shown in Figures S1, S2, and S3, respectively (in the supplementary file). The isotherms of the copper(II), lead(II), and copper-lead mixture adsorption are shown in Figures 8a, 8b, and 8c. Figure S1 was essential for determining the values of the Freundlich parameters; Figure S2 was used to establish them for the Langmuir parameters; and Figure S3 was used for the values of the Temkin parameters. The numerical values associated with each parameter of the models examined are grouped on Table 4. From the data presented, we found that the sorption processes followed the Langmuir model (Table 4). Indeed, it was found that, in the study of various processes, Regression coefficients generated by the Langmuir model were clearly superior than those of the other models considered. Moreover, the maximum adsorbed quantity (q_{max}) was practically similar to the experimental optimal sorption capacity (q_{exp}). The presence of an extended plateau also demonstrates that adsorption occurs on a uniform monolayer surface (Figures 8a, 8b, and 9c). It should be noted that the previously mentioned observations and hypotheses were made during the adsorption of ions on different materials, such as blast furnace slags, ligand-bound materials, carbon nanomaterial-based aerogels, and pretreated kaolin [6,7,10,17,49]. Furthermore, the type of adsorption process was defined by evaluating the R_L (Langmuir parameter) as a function of the initial concentration. The value of this parameter is of great importance for evaluating the quality of adsorption. Effectively, it has been cited that sorption is considered favorable if the R_L value is in the range of 0 to 1, while if the R_L value exceeds 1, adsorption is considered disadvantageous. Moreover, it is linear if the value of R_L corresponds to 1 [5,14,52]. The separation factor was determined using equation 7.

$$R_L = \frac{1}{1+C_0 b} \quad (7)$$

Where R_L, indicates the quality of the adsorption, b: Langmuir isotherm constant and C_0: initial concentration of the solution (mg/L).

Table 4. Characteristics of the analyzed isothermal models

Models	Parameters	Ads. Cu(II)	Ads. Pb(II)	Ads.Cu-Pb
Freundlich	k_F $(mg.g^{-1})(ml.mg^{-1})^{1/n}$	30.98	21.88	15.81
	1/n	0.31	0.36	0.4
	R^2	0.912	0.911	0.904
Langmuir	q_{exp} (mg/g)	124.87	115.14	108.47
	q_{max} (mg/g)	123.45	116.27	109.89
	k_L $(L.mg^{-1})$	0.135	0.088	0.053
	R^2	0.996	0.997	0.997
Temkin	b_T (kJ/mol)	0.110	0.101	0.098
	A_T (L/g)	2.82	1.09	1.8
	R^2	0.923	0.944	0.966

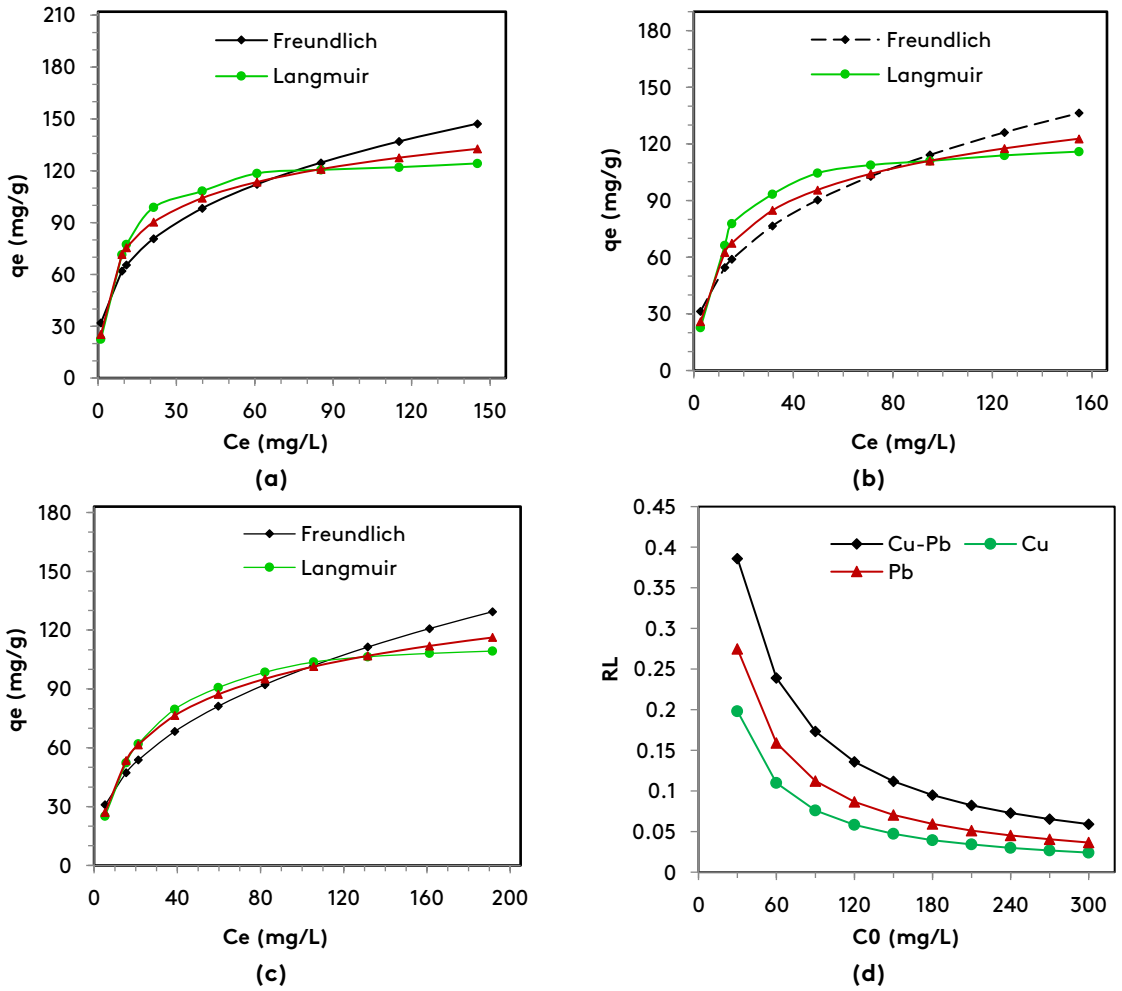

Fig. 8. (a) Curves of the adsorption isotherms for the copper adsorption on HZ, (b) Curves of the adsorption isotherms for the lead adsorption on HZ, (c) Curves of the adsorption isotherms for the copper-lead adsorption on HZ, (d) Influence of the initial concentration on the evolution of R_L.

From Figure 8(d), it was noticed that the value of R_L decreased with the intensification of the preliminary concentration of the solution in the three processes accomplished. The separation factor decreased from 0.198 to 0.024 during Cu(II) adsorption, from 0.274 to 0.036 during Pb(II) adsorption, and from 0.386 to 0.059 during Cu-Pb mixture adsorption (Figure 6c). Referring to these data, we could conclude that zeolite (HZ) favorably adsorbed the examined pollutants. The heterogeneity factor value (1/n) also reaffirmed that the removal of Cu(II), Pb(II), and Cu-Pb mixture by HZ is favorable, considering its value between 0 and 1 [7,22,52]. The Temkin model parameter (b_T) revealed that the removal of Cu(II), Pb(II), and Cu-Pb mixture is physical adsorption, since its value was less than 8 kJ/mol (Table 3) [52].

3.10 Kinetics of adsorption

Adsorption kinetics of Cu(II), Pb(II) and Cu-Pb mixture on HZ zeolite were studied using appropriate mathematical models, namely the pseudo-first order model (PFO), the pseudo-second order model (PSO), the model dedicated to external diffusion (ED), and Weber-Morris model (IPD) [22]. PFO , PSO, ED, and IPD are represented by equations 8-11, respectively.

$$\log(q_e - q) = -k_1 t + log q_e \quad (8)$$

$$\frac{t}{q} = \frac{1}{k_2 q_e^2} + \frac{t}{q_e} \quad (9)$$

$$log C_e = k_3 t + C_{Ex} \quad (10)$$

$$q = k_4 \sqrt{t} + C_{In} \quad (11)$$

Where Ce: equilibrium concentration (mg/L), qe and q: experimental adsorption capacity and calculated adsorption capacity at time t (mg/g), k_1: pseudo-first-order constant (min^{-1}), k_2: pseudo second order constant (g/mg min), k_3: external diffusion constant (min^{-1}), k_4: internal diffusion constant (mg/m. min ½), and (C_{In}) and (C_{Ex}) represent the intercepts.

Figures 9a and 9b display the plots of equations 8 and 9, while figures 10a and 10b show the plots of equations 10 and 11. Table 5 illustrates the parameters of the pseudo-order models, while the diffusion models are collected in Table 6.

According to Table 5, the correlation coefficients seem more relevant for the PSO ($R^2 \geq 0.991$) in the three processes studied. In addition, the maximum adsorbed capacity obtained by the PSO model is practically equivalent to the maximum quantity adsorbed experimentally in the different processes accomplished. These data made it possible to conclude that the sorption of copper, lead, and the copper-lead mixture in solution on HZ synthesized from blast furnace slag is pseudo-second-order kinetics. Comparable results and similar conclusions have been reported in previous studies, including the copper adsorption by chlorella pyrenoidosa [1], the copper and lead adsorption on treated blast furnace slag [6,7], cobalt adsorption by oxalated blast furnace slag [28], cadmuim adsorption onto NaOH-treated oil palm empty fruit bunch [38], and the Cr (VI) adsorption using natural Akadama clay [41] It should be noted that the values of the PSO model constant (k_2) demonstrated that HZ preferentially and successively adsorbs Cu (II), Pb (II), and Cu-Pb [60].

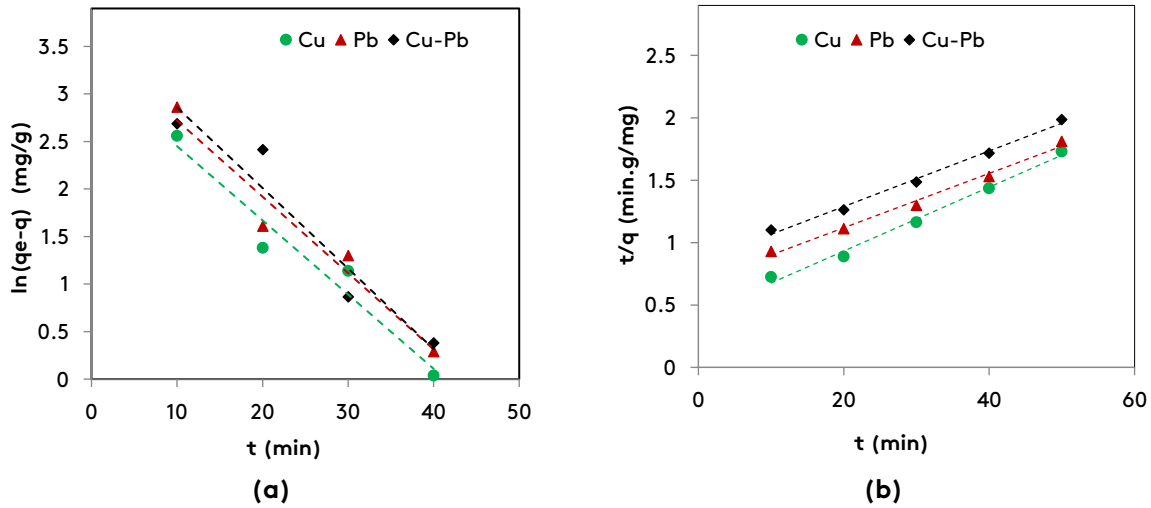

Fig. 10. Adsorption kinetics (a) Graphical description of PFO model, (b) Graphical description of PSO model

According to Figure 10a, the curves obtained from the equation describing external diffusion are linear straight lines, and according to Table 6, the correlation coefficients of these straight lines are greater than 0.98. From these data, we can conclude that the elimination by adsorption of pollutants studied on HZ is controlled by external diffusion under the effect of agitation [6,23].

Table 5. Kinetic parameters of pseudo-order models

Models	Parameters	Ads. Cu(II)	Ads. Pb(II)	Ads. Cu-Pb
PFO	qe (mg/g)	28.89	27.31	24.66
	q(mg/g	24.33	33.91	40.65
	K_1, min^{-1}	0.076	0.08	0.084
	R^2	0.954	0.951	0.921
PSO	qe (mg/g)	28.89	27.31	24.66
	q (mg/L	29.41	27.02	24.39
	K_2, g/mg min	0.034	0.037	0.041
	R^2	0.991	0.990	0.992

In Figure 10b, it was noted that the curves derived from equation (11) exhibit a multilinear appearance and do not cross the origin, indicating that they do not fit the criteria established by Weber and Morris [5]. This observation suggests the presence of different mechanisms controlling adsorption, with each straight segment representing a particular mechanism [52]. The first segment describes the movement of the studied ions from the solution to the boundary layer by an external diffusion process, while the second segment illustrates the progressive transfer of the examined ions from the HZ adsorbent surface to the internal pores through intraparticle diffusion. It is noted that the process reaches a steady state and stops when the HZ adsorption surface is saturated, due to the unavailability of activated adsorption sites. From Table 6, it was observed that the rate constants of the IPD model at the first stage surpass those of the second stage for all the processes analyzed. Indeed, the presence of active adsorption sites facilitates and intensifies the mass diffusion. It was also found that the intercept C_{In} for the adsorption of copper is more important, which reveals that the adsorbent examined demonstrates more affinity for copper [22].

Table 6. Kinetic parameters of diffusion models

Models	Parameters	Ads. Cu(II)	Ads. Pb(II)	Ads. Cu-Pb
ED	C_{Ex}	3.517	3.440	3.406
	K_3, min^{-1}	0.069	0.071	0.109
	R^2	0.991	0.987	0.980
IPD	1st linear part			
	C_{In}	12.63	11.33	10.79
	K'_4, mg/g.min	6.44	6.29	6.14
	R^2	0.99	0.99	0.99
	2nd linear part			
	C_{In}	15.72	14.59	13.98
	K''_4, mg/g.min	2.27	1.84	1.72
	R^2	0.98	0.97	0.95

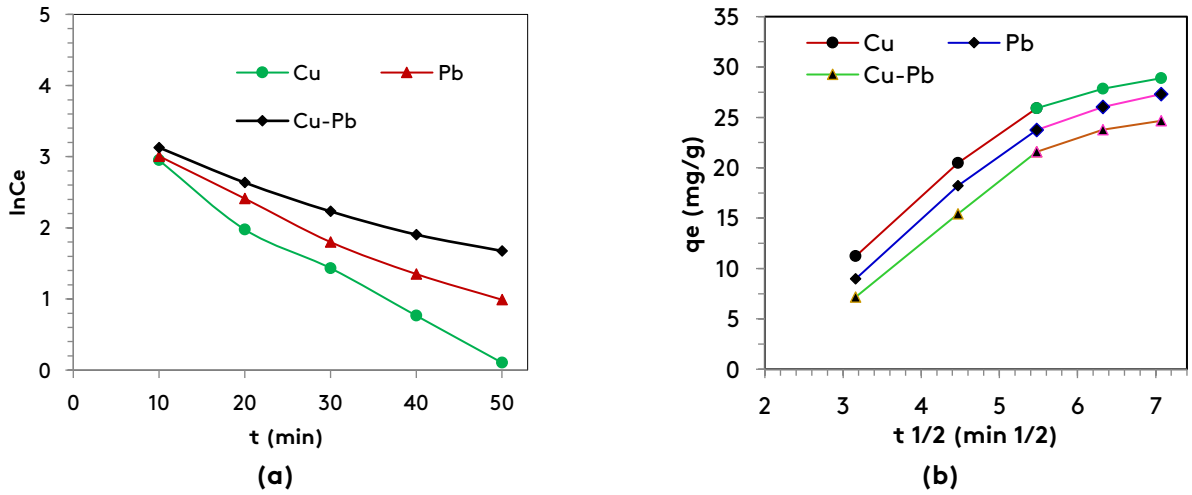

Fig. 10. Adsorption mechanism (a) external diffusion, (b) intraparticle diffusion

Considering these data, it was confirmed that the removal of the pollutants analyzed by adsorption on HZ is not completely regulated by intraparticle diffusion [7,60,61] From these outcomes, we can deduce that the overall adsorption rate of copper, lead, and copper-lead mixtures in solution on HZ is mainly influenced by external diffusion, followed by intraparticle diffusion [6,52,60,61].

3.11 Thermodynamic study

With the aim of establishing the nature of the processes undertaken and explaining the reaction interactions between the pollutants studied and the adsorbent surface of the HZ, we conducted a precise thermodynamic study. Gibbs free energy (ΔG°), entropy (ΔS°), and enthalpy (ΔH°) were the indicator parameters. They were determined based on equations 12-14 [14,39,61].

$$\Delta G^0 = -RT\ln k_d \quad (12)$$

$$\ln k_d = \frac{\Delta H^0}{R} \times \frac{1}{T} + \frac{\Delta S^0}{R} \quad (13)$$

$$k_d = \frac{C_i - C_e}{C_e} \times \frac{V}{M} = \frac{q_e}{C_e} \quad (14)$$

Where ΔG°: Gibbs free energy (kJ/mol), ΔS°: entropy (J/mol.K), ΔH°: enthalpy (kJ/mol), R: the universal gas constant (8.314 J/mol K), T: absolute temperature (K) and K_d: distribution coefficient (L/g),

The graphical representation of $\ln k_d$ as a function of 1/T is reproduced in Figure 11. The values of ΔG°, ΔS°, ΔH°, and k_d are cited in Table 7. Figure 11 revealed a very high correlation between the Van't Hoff model (equation 11) and experimental results ($R^2 \geq 0.991$) (Table 6). Furthermore, we observed a decrease in the K_d value (Table 7), which indicated that the increase in temperature weakened the distribution of copper, lead, and copper-lead mixture on the HZ zeolite surface [6,52]. Regardless of the solution temperature, the K_d values indicate that the HZ zeolite has a stronger attraction for Cu(II) ions than for Pb(II) ions, because the distribution coefficient K_d for the adsorption of Cu(II) is always higher than that of lead adsorption [20,27,52].

Table 7. Thermodynamic parameters

Ions	*T, (K)*	*ΔG°, kJ/mol*	*ΔH°, kJ/mol*	*ΔS°, J/mol.K*	*K_d, L/g*
Cu(II)	293	-17.81	-6.07	-17.46	1.46
	308	-18.46			1.32
	318	-18.85			1.22
	328	-19.21			1.12
Pb(II)	293	-17.35	-5.61	-16.39	1.21
	308	-17.99			1.10
	318	-18.39			1.02
	328	-18.75			0.94
Cu- Pb	293	-14.41	-4.65	-20.54	0.82
	308	-15.01			0.75
	318	-15.66			0.69
	328	-16.01			0.64

It appears from Table 7 that the sorption of copper, lead and the mixture on the HZ zeolite is exothermic, as evidenced by the negative enthalpy values [24]. Furthermore, based on these values (ΔH° ≤ 40 kJ/mol), we were able to confirm that copper, lead, and copper-lead ions are removed by physical adsorption [23,62]. The negativity of entropy clearly proved a decrease in disorder at the interface of synthetic zeolite (HZ) and metal ions in solution. The reduction in disordered movements at the interface between the adsorbent and the adsorbate could be due to a good correlation between the pollutants analyzed and the surface of HZ [52]. The ΔG° values revealed that the adsorption processes carried out were spontaneous [1,61]. The Gibbs energy, whose value is between -20 and 0 kJ/mol, suggests that the removal of pollutants was carried out via a physical adsorption process [5,6]. The effect of the increase in solution temperature on the regression of ΔG° highlights that mass transfer is inversely related to the temperature of the medium [1].

3.12 Desorption process

Recovery of toxic pollutants from the loaded sorbent is essential to ensure its reuse and to prevent the formation of contaminated solid waste which, once regenerated, can cause another form of pollution. Given this context, we accomplished the desorption of copper from the preloaded HZ, knowing that the desorption efficiency was established using equation 15.

$$\text{Desorption rate} = \frac{q_{des}}{q_{ads}} \times 100 \quad (15)$$

Where (q_{ads}) represents adsorbed quantity at equilibrium (mg/g) for cycle I and (q_{ads}) desorbed quantity at equilibrium (mg/g).

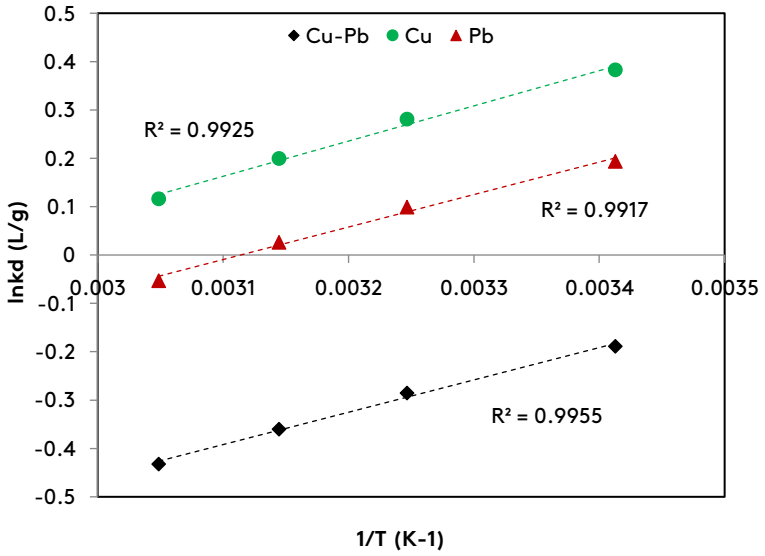

Fig. 11. Progression of ln(k_d) with inverse temperature (T^{-1}): Van't Hoff presentation

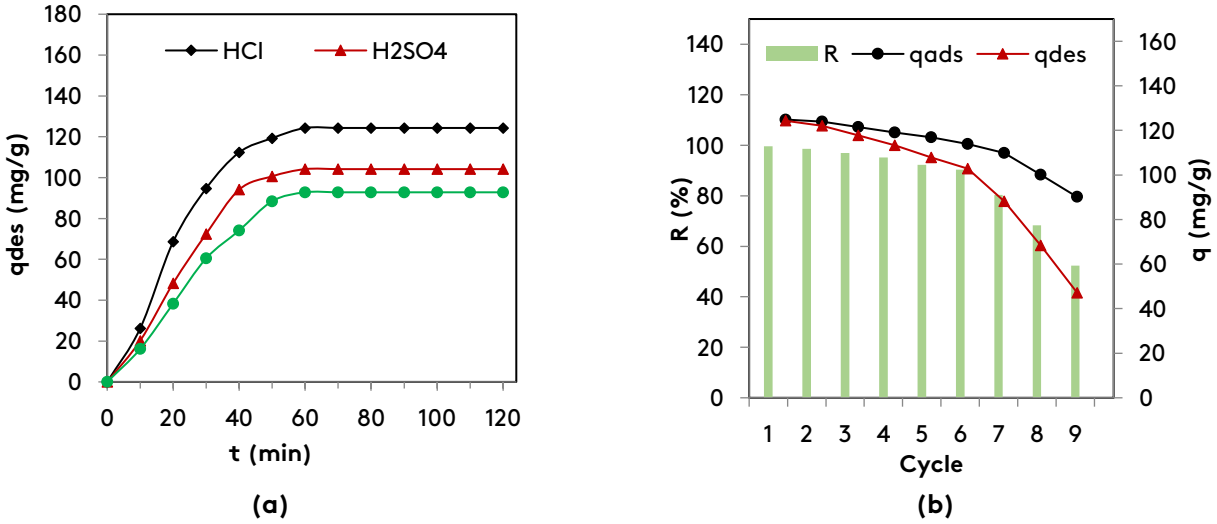

Fig. 12. (a) Desorption kinetics, (b) desorption cycles desorption

The kinetics and cycles of the adsorption and desorption of copper are illustrated in Figure12. From our experiments, the HCl eluent was found to be more effective in desorbing copper from saturated HZ, as shown in Figure 12(a). The high polarity and low viscosity of HCl had a significant impact in this process [5]. Due to the high concentration of protons in the solution, the negatively charged HZ surface had to reverse its sign, which caused the release of copper ions [52]. From Figure 12(b), it is evident that the HZ can be operated after 6 consecutive cycles. The decrease observed from the seventh cycle was probably caused by adsorbent depletion and material loss [5,63].

4. Conclusion

This research revealed that HZ designed from treated steel slag (TBFS) is an efficient adsorbent for removing Cu(II), Pb(II) and Cu-Pb ions in solution by adsorption in batch mode. Further analysis of synthetic HZ using XRF and XRD revealed its main composition, which is dominated by sodium oxide (27.11%), followed by silicon dioxide (20.74%), aluminum oxide (15.78%), calcium oxide (11.64%), and phosphorus hemi-pentoxide (7.27%). The zeolite obtained from TBFS corresponds to a hydroxyapatite (HZ) zeolite, according to the analyses of the Ca/P, Na/Al, and Si/Al ratios. The analyses undertaken on the HZ also

revealed a specific surface area of 409.63 m²/g and a zero charge point (PZC) estimated at 3.6 on the pH scale. The effect of contact time demonstrated that the adsorption processes carried out managed to reach equilibrium within 50 minutes. The adsorbed quantity of Cu(II), Pb(II), and Cu-Pb on HZ reached its maximum value after optimization of the determining factors (tc = 50 min, ms= 1 g, V_{ag} = 200 rpm, pH = 5, T = 20 °C, Øs = 250 µm, and C_0= 240 mg/L). The maximum sorption capacity of copper, lead, and copper-lead mixture is estimated at 123.45, 116.27, and 108.89 mg/g, respectively. Analysis of adsorption isotherms demonstrated that the Langmuir model best described the adsorption processes, emphasizing that adsorption occurred on a homogeneous monolayer surface. The values obtained for the heterogeneity factor (1/n) and the separation factor (R_L) proved that the considered adsorption processes are favorable, while the values of the Temkin isotherm constant (bt) revealed that the removal of copper, lead, and copper-lead was accomplished by physical adsorption. Kinetic analyses proved that the adsorption of copper, lead, and copper-lead on HZ followed a pseudo-second-order model, and their removal processes are controlled by external diffusion generated by agitation as well as by internal diffusion caused by the diffusional regime. The values of the calculated thermodynamic parameters proved that the adsorption processes carried out are spontaneous, exothermic, and less entropic, and they highlighted that the removal of the ions examined by HZ in solution was accomplished by physical adsorption under the influence of electrostatic attractions. The desorption test confirmed that HZ could be reliably reused for 6 consecutive cycles in the presence of hydrochloric acid (HCl, 0.05 M) as eluent. To summarize, the use of HZ as an adsorbent proves to be both easy and convenient. Moreover, this option proves to be more economically beneficial than commercially available adsorbents. It is with this objective that we propose an efficient and reliable adsorption solution to remove copper and lead from wastewater.

References

[1] Sharififard, H. (2018). Statistical physics modeling of equilibrium adsorption of cadmium ions onto activated carbon, chitosan and chitosan/activated carbon composite. *Advances in Environmental Technology*, *2*, 149-154. https://doi.org/10.22104/aet.2019.2619.1132

[2] Wang, Z., Liu, J., Yang, Y., Yu, Y., Yan, X., Zhang, Z. (2020).AMn_2O_4 (A=Cu, Ni and Zn) sorbents coupling high adsorption and regeneration performance for elemental mercury removal from syngas. *Journal of Hazardous Materials*, *388*, 121738. https://doi.org/10.1016/j.jhazmat.2019.121738

[3] Abdullah, N., Yusof, N., Lau, W.J., Jaafar, J., Ismail, A.F. (2019). Recent trends of heavy metal removal from water/wastewater by membrane technologies. *Journal of Industrial and Engineering Chemistry*, *76*, 17-38. https://doi.org/10.1016/j.jiec.2019.03.029

[4] Badvi Loulic, F., Shirazi, R.H.S.M., Miralinaghi, M., Ahmad Panahi, H, Moniri, E. (2023). Highly efficient removal of toxic As(V), Cd (II), and Pb(II) ions from water samples using $MnFe_2O_4$@SBA-15-$(CH_2)_3$-adenine as a recyclable bio-nanoadsorbent. *Microporous and Mesoporous Materials*, *356*, 112567. https://doi.org/10.1016/j.micromeso.2023.112567

[5] Chouchane, T., Boukari, A. (2022). Impact of Influencing Parameters on the Adsorption of nickel by kaolin in an aqueous medium. *Analytical and Bioanalytical Chemistry Research*, *9*, 381-399. https://doi.org/10.22036/ABCR.2022.325691.1716

[6] Chouchane, T., Boukari, A., Khireddine, O., Chibani, S., Chouchane, S. (2023). Cu(II) removal from aqueous medium using blast furnace slag (BFS) as an effective adsorbent. *Eurasian Journal of Chemistry, 110*(2), 115-130. https://doi.org/10.31489/2959-0663/2-23-3

[7] Chouchane, T., Chibani, S., Khireddine, O., Boukari, A. (2023). Adsorption study of Pb(II) ions on the blast furnace slag (BFS) from aqueous solution. *Iranian Journal of Materials Science and Engineering*, *20*, 1-13. https://doi.org/10.22068/ijmse.3011

[8] Rezaei, M., Panahi, H. A., Nasrollahi, S., Moniri, E., Torabi Fard, N. (2023). Synthesis and characterization of zinc oxide nanoparticles grafted poly [(N, N-

Dimethylacrylamide)-co-(Allyl Acetoacetate)] for removal of Pb (II) in environmental and biological samples. *Separation Science and Technology*, *58*(8), 1516-1526. https://doi.org/10.1080/01496395.2023.2195081

[9] Panahi, H.A., Abdouss, M., Ghiabi, F., Moniri, E., Mousavi Shoushtari, A. (2011). Modification and characterization of poly (ethylene terephthalate)-grafted-acrylic acid/acryl amide fiber for removal of lead from human plasma and environmental samples. *Journal of Applied Polymer Science*, *124*, 5236-5246. https://doi.org/10.1002/app.34224

[10] Awual, M.R., (2019). Mesoporous composite material for efficient Pb(II) detection and removal from aqueous media. *Journal of Environmental Chemical Engineering*, *7*, 103124. https://doi.org/10.1016/j.jece.2019.103124

[11] Betiha, M.A., Moustafa, Y.M., El-Shahat, M.F., Rafik, E. (2020). Polyvinylpyrrolidone-aminopropyl-SBA-15 schiff base hybrid for efficient removal of divalent heavy metal cations from wastewater. *Journal of Hazardous Materials*, *397*, 122675. https://doi.org/10.1016/j.jhazmat.2020.122675

[12] Kainth, S., Sharma, P., Pandey, O.P. (2012). Green sorbents from agricultural wastes: A review of sustainable adsorption materials. *Applied Surface Science Advances*, *19*, 100562. https://doi.org/10.1016/j.apsadv.2023.100562

[13] Huang, W-H., Wu, R-M., Chang, J-S., Juang, S-Y., Lee, D-J. (2023). Manganese ferrite modified agricultural waste-derived biochars for copper ions adsorption. *Bioresource Technology*, *367*, 128303. https://doi.org/10.1016/j.biortech.2022.128303

[14] Obayomi, K.S., Auta, M. (2019). Development of microporous activated aloji clay for adsorption of Pb(II) (II) ions from aqueous solution. *Heliyon*, 5, e02799. https://doi.org/10.1016/j.heliyon.2019.e02799

[15] Ben Ali, M., Wang, F., Boukherroub, R., Lei, W., Xia, M. (2019). Phytic acid-doped polyanilinenanofibers-clay mineral for efficient adsorption of copper (II) ions. *Journal of Colloid and Interface Science*, *553*, 688-698. https://doi.org/10.1016/j.jcis.2019.06.065

[16] Chen, W., Lu, Z., Xiao, B., Gu, P., Yao, W., Xing, J., Asiri, A.M., Alamry, K.A., Wang, X., Wang, S. (2019). Enhanced removal of Pb(II) ions from aqueous solution by iron oxide nanomaterials with cobalt and nickel doping. *Journal of Cleaner Production*, *211*, 1250-1258. https://doi.org/10.1016/j.jclepro.2018.11.254

[17] Smith, M., Hamwi, B., Rogers, R.E. (2022). Carbon nanomaterial-based aerogels for improved removal of copper(II), zinc(II), and lead(II) ions from water. *Environmental Science Advances*, *1*, 208-215. https://doi.org/10.1039/d2va00049k

[18] Wang, H., Shang, H., Sun, X., Hou, L., Wen, M., Qiao, Y. (2019). Preparation of thermo-sensitive surface ion-imprinted polymers based on multi-walled carbon nanotube composites for selective adsorption of Pb(II) ion. *Colloids and Surfaces A: Physicochemical and Engineering Aspects*, *585*, 124139. https://doi.org/10.1016/j.colsurfa.2019.124139

[19] Rong, M., Xu, X., Wang, K., Lu, L., Bai, Y., Tian, Y., Hou, Z., Zhao, R., Ma, Y., Jiang, Y. (2023). A novel hydroxyapatite-based hollow microsphere nanocomposite for copper ion adsorption. *Chemical Physics Letters*, *585*, 140548. https://doi.org/10.1016/j.cplett.2023.140548

[20] Alkherraz, A.M., Ali, A.K., Elsherif K.M. (2020). Removal of Pb(II), Zn(II), Cu(II) and Cd(II) from aqueous solutions by adsorption onto olive branches activated carbon: equilibrium and thermodynamic studies. *Chemistry Internationnal*, 6, 11-20. https://doi.org/10.5281/zenodo.2579465

[21] Tauetsile, P.J., Oraby, E.A., Eksteen, J.J. (2018). Adsorption behaviour of copper and gold Glycinates in alkaline media onto activated carbon. Part 2, Kinetics. *Hydrometallurgy*, *178*, 195-201. https://doi.org/10.1016/j.hydromet.2018.04.016

[22] Chouchane, T., Khireddine, O., Boukari, A. (2021). Kinetic studies of Ni(II) ions adsorption from aqueous solutions using the blast furnace slag (BF slag). *Journal of Engineering and Applied Science*, *68*, 34. https://doi.org/10.1186/s44147-021-00039-3

[23] Chouchane, T., Boukari, A., Khireddine, O., Chibani, S., Chouchane, S. (2023). Equilibrium, kinetics, and thermodynamics of batch adsorption of Mn(II) ions on blast furnace slag (BFS) and kaolin (KGA). *Journal of Engineering and Applied Science*, *70*, 58. https://doi.org/10.1186/s44147-023-00218-4

[24] Chouchane, T., Khireddine, O., Chibani, S., Boukari, A. (2023). Removal of Cr(III), Pb(II) and Cr-Pb Mixture by Blast Furnace Slag (BFS) in Solution. *Analytical and Bioanalytical Chemistry Research*, *10*, 251-268. https://doi.org/10.22036/ABCR.2022.365182.18

[25] Li, C.X., Zhang, Q.W., Li, L. (2021) Synthesis of NaA zeolite from blast furnace slag (BFS) and Its utilization for adsorption of basic dye (methylene blue). *Journal of Physics: Conference Series, 2224*, 012068. https://doi.org/10.1088/1742-6596/2224/1/012068

[26] Dhmees, A.S., Klaleel, N.M., Mahoud, S.A. (2018). Synthesis of silica nanoparticles from blast furnace slag as cost-effective adsorbent for efficient azo-dye removal. *Egyptian Journal of Petroleum*, *27*, 1113-1121. https://doi.org/10.1016/j.ejpe.2018.03.012

[27] Xue, Y., Wu, S., Zhou, M. (2013). Adsorption characterization of Cu(II) from aqueous solution onto basic oxygen furnace slag. *Chemical Engineering Journal, 231*, 355-364. https://doi.org/10.1016/j.cej.2013.07.045

[28] Le, Q.T.N., Vivas, E.L., Cho, K. (2021). Oxalated blast-furnace slag for the removal of cobalt(II) ions from aqueous solutions. *Journal of Industrial and Engineering Chemistry*, *95*, 57-65. https://doi.org/10.1016/j.jiec.2020.12.003

[29] Yamaguchi, S., Hongo, T. (2021). Synthesis of metaettringite from blast furnace slag and evaluation of its boron adsorption ability. *Environmental Science and Pollution Research*, *28*, 15070-15075. https://doi.org/10.1007/s11356-020-11028-z

[30] Piatak, N.M., Seal, R.R., Hoppe, D.A., Green, C.J., Buszka, P.M. (2019). Geochemical characterization of iron and steel slag and its potential to remove phosphate and neutralize acid. *Minerals*, *9*, 468. https://doi.org/10.3390/min9080468

[31] Zuo, M., Renman, G., Gustafsson, J.P., Klysubun, W. (2018). Phosphorus removal by slag depends on its mineralogical composition: a comparative study of aod and eaf slags. *Journal of Water Process Engineering*, *25*, 105-112. https://doi.org/10.1016/j.jwpe.2018.07.003

[32] Navarro, C., Díaz, M., Villa-García, M.A. (2010). Physico-chemical characterization of steel slag. study of its behavior under simulated environmental conditions. *Environmental Science & Technology*, *44*(14), 5383-5388. https://doi.org/10.1021/es100690b

[33] Li, C., Li, X., Yu, Y., Zhang, Q., Li, L., Zhong, H., Wang, S. (2022). Novel conversion for blast furnace slag (BFS) to the synthesis of hydroxyapatite-zeolite material and its evaluation of adsorption properties. *Journal of Industrial and Engineering Chemistry*, *105*, 63-73. https://doi.org/10.1016/j.jiec.2021.08.017

[34] Basaleh, A.A., Al-Malack, M.H., Saleh, T.A. (2021). Poly(acrylamide acrylic acid) grafted on steel slag as an efficient magnetic adsorbent for cationic and anionic dyes. Journal of *Environmental Chemical Engineering*, *9*, 105126. https://doi.org/10.1016/j.jece.2021.105126

[35] Brunauer, S., Emmett, P.H., Teller, E. (1938). Adsorption of gases in multimolecular layers. *Journal of the American Chemical Society*, *60*, 309-319. https://doi.org/10.1021/ja01269a023

[36] Li, C., Zhong, H., Wang, S., Xue, J.R., Zhang, Z.Y. (2015). A novel conversion process for waste residue: Synthesis of zeolite from electrolytic manganese residue and its application to the removal of heavy metals. *Colloids and Surfaces A: Physicochemical and Engineering Aspects*, *470*, 258-267. https://doi.org/10.1016/j.colsurfa.2015.02.003

[37] Murakami T., Sugano Y., Narushima T., Iguchi Y., Ouchi C. (2011). Recovery of calcium from BF slag and synthesis of zeolite A using its residue. *ISIJ International*, *51*, 901-905. https://doi.org/10.2355/isijinternational.51.901

[38] Mustapha, L.S., Yusuff, A.S., Dim, P.E. (2023). RSM optimization studies for cadmium ions adsorption onto pristine and acid-modified kaolinite clay. *Heliyon*, *9*(8), e18634. https://doi.org/10.1016/j.heliyon.2023.e18634

[39] Hussain, N., Chantrapromma, S., Suwunwong, T., Phoungthong, K. (2020). Cadmium (II) removal from aqueous solution using magnetic spent coffee ground biochar: kinetics, isotherm and thermodynamic adsorption. *Materials Research Express*, *7*, 085503. https://doi.org/10.1088/2053-1591/abae27

[40] Mustapha, S., Ndamitso, M.M., Abdulkareem, A.S., Tijani, J.O., Mohammed, A.K., Shuaib, D.T. (2019). Potential of using kaolin as a natural adsorbent for the removal of pollutants from tannery wastewater. *Heliyon*, *5*, e02923. https://doi.org/10.1016/j.heliyon.2019.e02923

[41] Zhao, Y., Yang, S., Ding, D., Chen, J., Yang, Y., Lei, Z., Feng, C., Zhang, Z. (2013). Effective adsorption of Cr (VI) from aqueous solution using natural Akadama clay. *Journal of colloid and interface science*, *395*, 198-204. https://doi.org/10.1016/j.jcis.2012.12.054

[42] Foroutan, R., Mohammadi, R., Farjadfard, S., Esmaeili, H., Ramavi, B., Sorial, G.A. (2019). Eggshell nano-particle potential for methyl violet and mercury ion removal: surface study and field application. *Advanced Powder Technology*, *30*, 2188-2199. https://doi.org/10.1016/j.apt.2019.06.034

[43] Simha, P., Banwasi, P., Mathew, M., Ganesapillai, M. (2016). Adsorptive resource recovery from human urine: system design, parametric considerations and response surface optimization. *Procedia Engineering*, *148*, 779-786. https://doi.org/10.1016/j.proeng.2016.06.557

[44] Gupta, A., Balomajumder, C. (2017). Statistical optimization of process parameters for thesimultaneous adsorption of Cr (VI) and phenol onto Fe-treated tea waste biomass. *Applied Water Science*, *7*, 4361-4374. https://doi.org/10.1007/s13201-017-0582-9

[45] Yogeshwaran, V., Priya, A.K. (2021). Adsorption of lead ion concentration from the aqueous solution using tobacco leaves. *Materials Today: Proceedings*, *37*, 489-496. https://doi.org/10.1016/j.matpr.2020.05.467

[46] Karami, K., Beram, S.M., Bayat, P., Siadatnasab, F., Ramezanpour, A. (2022). A novel nanohybrid based on metal–organic framework MIL101-Cr/PANI/Ag for the adsorption of cationic methylene blue dye from aqueous solution. *Journal of Molecular Structure*, *1247*, 131352. https://doi.org/10.1016/j.molstruc.2021.131352

[47] Du, P., Zhang, J., Cai, Z., Ge, F. (2023). High adsorption of cationic dyes from aqueous solution using worm-like porous nanosilica: Isotherm, kinetics and thermodynamics. *Materials Today Communications*, *35*, 105697. https://doi.org/10.1016/j.mtcomm.2023.105697

[48] Zhao, H., Ouyang, X.K., Yang, L.Y. (2021). Adsorption of lead ions from aqueous solutions by porous cellulose nanofiber–sodium alginate hydrogel beads. *Journal of Molecular Liquids*, *324*, 115122. https://doi.org/10.1016/j.molliq.2020.115122

[49] Chouchane, T., Yahi, M., Boukari, A., Balaska, A., Chouchane, S. (2016). Adsorption of the copper in solution by the kaolin. *Journal of Materials and Environmental Science, 7*, 2825-2842. http://www.jmaterenvironsci.com/Document/vol7/vol7_N8/295-JMES-1856-Chouchane.pdf

[50] Jiang, S., Huang, L., Nguyen, T.A.H., Sik, O.k. Y., Rudolph, V., Yang, H. , Zhang D. (2016). Copper and zinc adsorption by softwood and hardwood biochars under elevated sulphate-induced salinity and acidic pH conditions. *Chemosphere*, *142*, 64-71. https://doi.org/10.1016/j.chemosphere.2015.06.079

[51] Iqbal, J., Wattoo, F.H., Wattoo, M.H.S., Malik, R., Tirmizi, S.A., Imran, M., Ghangro A.B. (2011). Adsorption of acid yellow dye on flakes of chitosan prepared from fishery wastes. *Arabian Journal of Chemistry*, *4*, 389-395. https://doi.org/10.1016/j.arabjc.2010.07.007

[52] Chouchane, T., Abedghars, M.T., Chouchane, S., Boukari, A. (2024). Improvement of the sorption capacity of methylene blue dye using

slag, a steel by product. *Kuwait Journal of Science*, *51*, 100210. https://doi.org/10.1016/j.kjs.2024.100210

[53] Wekoye, J.N., Wanyonyi, W.C., Wangila, P.T., Tonui, M.K. (2020). Kinetic and equilibrium studies of congo red dye adsorption on cabbage waste powder. *Environmental Chemistry and Ecotoxicology*, *2*, 24-31. https://doi.org/10.1016/j.enceco.2020.01.004

[54] Cherono, F., Mburu, N., Kakoi B. (2021). Adsorption of lead, copper and zinc in a multi-metal aqueous solution by waste rubber tires for the design of single batch adsorber. *Heliyon*, *7*, e08254. https://doi.org/10.1016/j.heliyon.2021.e08254

[55] Chouchane, T., Chouchane, S., Boukari, A., Mesalhi, A. (2015). Adsorption of binary mixture lead nickel by kaolin. *Journal of Materials and Environmental Science*. *6*, 924-941.

[56] Goel, J., Kadirvelu, K., Rajagopal, C. (2004). Competitive sorption of Cu(II), Pb(II) and Hg(II) ions from aqueous solution using coconut shell-based activated carbon. *Adsorption Science & Technology*, *22*, 257-273. https://doi.org/10.1260/02636170415034

[57] Gupta N., Sen R. (2017). Kinetic and equilibrium modelling of Cu (II) adsorption from aqueous solution by chemically modified Groundnut husk (Arachishypogaea). *Journal of Environmental Chemical Engineering*. *5*, 4274-4281. https://doi.org/10.1016/j.jece.2017.07.048

[58] Jiang, S., Huang, L., Nguyen, T.A.H., Sik, O.k.Y., Rudolph, V., Yang, H., Zhang D. (2016). Copper and zinc adsorption by softwood and hardwood biochars under elevated sulphate-induced salinity and acidic pH conditions. *Chemosphere*, *142*, 64-71. https://doi.org/10.1016/j.chemosphere.2015.06.079

[59] Aquino, R.R., Tolentino, M.S., Elacion, R.M.P.D., Ladrillono, R., Laurenciana, T.R.C., Basilia, B.A. (2019). Adsorptive removal of lead (Pb^{2+}) ion from water using cellulose acetate/polycaprolactone reinforced nanostructured membrane. *IOP Conference Series Earth and Environmental Science*, *191*, 012139. https://doi.org/10.1088/1755-1315/191/1/012139

[60] Yogeshwaran, V., Priya, A.K. (2021). Adsorption of lead ion concentration from the aqueous solution using tobacco leaves. *Materials Today: Proceedings*, *37*, 489-496. https://doi.org/10.1016/j.matpr.2020.05.467

[61] Raeia, B., Barekat, A., Shariatinia, H. (2019). Removal of Ni(II) from aqueous solution using modified MCM-41 nanoadsorbents. *Advances in Environmental Technology*, *3*, 157-169. https://doi.org/10.22104/aet.2020.4178.1207

[62] Sihag, S., Pal, J. (2023). Adsorption of fluoride ions from aqueous solution by rice husk based nanocellulose. *Advances in Environmental Technology*, *9*(3), 194-214. https://doi.org/10.22104/AET.2023.5963.1643

[63] Abdollah, F., Borghei, S.M., Moniri, E., Kimiagar, S., Panahi, H.A. (2019). Laser irradiation for controlling size of TiO_2–Zeolite nanocomposite in removal of 2,4-dichlorophenoxyacetic acid herbicide. *Water Science and Technology*, *80*, 864-873. https://doi.org/10.2166/wst.2019.333

How to site this paper:

Chouchane, T., Abedghars, M. T., Chouchane, S. & Boukari, A. (2024). Synthesis of hydroxyapatite-zeolite from blast furnace slag and its application for the removal of copper, lead and copper-lead mixture by adsorption. Advances in Environmental Technology, 10(4), 339-359. doi: 10.22104/aet.2024.6914.1893